Coordinated changes in cell membrane and cytoplasm during maturation of apoptotic bleb

青木, 佳南

Coordinated changes in cell membrane and cytoplasm during maturation of apoptotic bleb

Kana Aoki

Graduate School of Systems Life Sciences, Kyushu University

Contents

Coordinated changes in cell membrane and cytoplasm during maturation of apoptotic bleb

Abstract

Apoptotic cells form membrane blebs, but little is known about how the formation and dynamics of membrane blebs are regulated. The size of blebs gradually increases during the progression of apoptosis, eventually forming large extracellular vesicles called apoptotic bodies that have immune-modulating activities. In this study, I investigated the molecular mechanism involved in the differentiation of blebs into apoptotic blebs by comparing the dynamics of the bleb formed during cell migration and the bleb formed during apoptosis. I revealed that the enhanced activity of ROCK1 is required for the formation of small blebs in the early phase of apoptosis, which leads to the physical disruption of nuclear membrane and the degradation of Lamin A. In the late phase of apoptosis, the loss of asymmetry in phospholipids distribution caused the enlargement of blebs, which enabled translocation of damage associated molecular patterns (DAMPs) to the bleb cytoplasm and maturation of functional apoptotic blebs. Thus, changes in cell membrane dynamics are closely linked to cytoplasmic changes during apoptotic bleb formation.

Introduction

Various intracellular changes occur over the course of apoptosis. Molecular mechanisms of nuclear condensation, genome fragmentation, and exposure of phosphatidylserine (PS) to the outer leaflet of plasma membrane during apoptosis have been studied intensively (1). The formation of plasma membrane blebs is an invariable characteristic of apoptosis but the knowledge of its molecular mechanism is limited (2). In the case of blebs that form during programmed necrosis, proteins that open pores in the cell membrane translocate to the plasma membrane where they enhance the permeability of the plasma membrane and cause the cell to rupture (3). However, it remains unclear how the interaction between the plasma membrane and actin cytoskeleton is regulated to form apoptotic membrane blebs. In this study, I investigated the molecular mechanisms of bleb formed during apoptosis (apoptotic bleb).

In previous studies, caspase-3 was shown to be essential in the formation of blebs during apoptosis, as caspase-3-deficient cells cannot form blebs (4, 5). Subsequently, it was shown that ROCK1 is cleaved and activated by caspase-3 during apoptosis (6, 7). Activation of ROCK1 by caspase-3 is Rho-independent and induces bleb formation by up-regulating contractility of the actomyosin cortex. The upregulation of the contractile force exerted by the actomyosin cortex increases the pressure inside the cell and leads to the detachment of the plasma membrane from the underlying actin cortex. The plasma membrane continues to expand as it detaches from the actin cortex, but the actin cortex is rapidly reassembled below the plasma membrane to halt bleb expansion, and eventually cause it to contract. Such expansion and contraction of blebs facilitate the packaging of cellular debris into apoptotic blebs, which function as damage associated molecular patterns (DAMPs), and promote the conversion of apoptotic blebs to apoptotic bodies (8).

Membrane blebs are observed not only in apoptosis but also in cytokinesis and cell movement (9). I previously identified molecular networks involved in the regulation of membrane blebs during cell migration (10). In particular, I revealed that two small G

proteins, Rnd3 and RhoA, are involved in the regulation of the actin cytoskeleton during bleb formation and regression (11).

However, it remains unclear whether apoptotic membrane blebs are controlled by the same molecular mechanism as blebs associated with cell migration. There are clear differences in the dynamics of blebs that form during cell migration and during apoptosis. The blebs of freely moving cells are generally of constant size, whereas those that form during apoptosis progressively increase in size with the maturation of apoptosis and eventually develop into apoptotic blebs containing DAMPs (12). However, how bleb dynamics are altered during apoptosis and contribute to the progression of apoptosis remains unclear. In the present study, I addressed this issue by combining experimental observations and mathematical simulation.

Results

The size of apoptotic blebs changes with the progression of apoptosis

I previously reported that the human colon cancer-derived DLD1 cells form blebs and migrate freely when seeded on collagen gel (10). I first established DLD1 cells stably expressing GFP-based fluorogenic caspase-3 reporter, FlipGFP(casp3)-T2A-mCherry (13) in order to demonstrate that treatment with anti-Fas antibody induce apoptosis of DLD1 cells. I confirmed that the activity of FlipGFP-based caspase-3 reporter was up-regulated only during apoptosis and not during cell migration (Fig.1A).

Next, I compared the morphology of blebs between migrating cells and apoptotic cells. While blebs associated with cell movement form at a constant speed and size apoptosis, the bleb dynamics and bleb size of apoptosis-associated blebs change over time (Figs.1B-1D, S1A). Specifically, in early stage apoptosis, small blebs with rapid regression speed are formed, and in late stage apoptosis, large blebs with slow regression speed are formed (Figs. 1B and 1D). As a result, the number of blebs formed during the defined time period (10 minutes) is greater in the early stage than in the later stage of apoptosis (Fig.1E).

Cells exhibit various changes over the course of apoptosis, such as the release of cytochrome c from mitochondria to the cytoplasm, the exposure of PS to the outer leaflet of plasma membrane and the cytoplasmic release of nuclear proteins including High Mobility Group Box 1 (HMGB1) (14). I first sought to determine whether the morphological changes of blebs are associated with specific intracellular changes. Bleb formation and cytochrome c release occur from the early stage of apoptosis (Fig. 1F), whereas exposure of PS and release of HMGB1 into the cytoplasm are observed only in the late stage of apoptosis (Figs. 1G and 1H). Furthermore, in the late stage of apoptosis, the nuclear membrane disappears by the cleavage of Lamin A by caspases (Fig. 1H) (15). These cellular changes are characteristic of apoptosis and are never observed in freely moving DLD1 cells (Figs. 1F and 1H).

What is the physiological significance of membrane blebbing in apoptosis? Addition of the ROCK inhibitor, Y-27632, to cells undergoing apoptosis suppresses the

formation of membrane blebs (12). I found that suppression of bleb formation during apoptosis by treatment with the ROCK inhibitor did not affect the exposure of PS to the outer leaflet of plasma membrane (Fig. 1G). However, interestingly, translocation of HMGB1 to the cytoplasm and formation of apoptotic body were completely suppressed (Figs. 1H and 1I).

Lamin A, one of the bona fide constituents of the nuclear envelope, is degraded by caspase during apoptosis. Therefore, I examined whether the suppression of bleb formation by ROCK1 inhibition during apoptosis affected the degradation of Lamin A. Lamin A was not degraded in migrating cells with blebs but was degraded in apoptotic cells as expected. Importantly, Y-27632 treatment significantly reduced the degradation of Lamin A compared to control apoptotic cells. This finding indicates that the caspase-mediated degradation of Lamin A and subsequent collapse of the nuclear envelope are enhanced as a direct consequence of increased acto-myosin contractility and membrane blebbing. (Figs.1J and 1K). Thus, repeated expansion and retraction of blebs is required to package cytoplasmic components into cell membrane protrusions. In particular, in order for Lamin A present inside of the nuclear membrane to be degraded by caspase activated in the cytoplasm, the nuclear membrane needs to be physically disrupted. Considering that nuclear membrane disruption did not occur when treated with Y-27632 (Fig. 1F), the formation of blebs in the early stages of apoptosis plays essential roles in the degradation of Lamin A and the formation of apoptotic blebs in the later stages of apoptosis by physically disrupting the nuclear membrane.

Localization of Rnd3 and RhoA in apoptotic blebs

The blebs that form at the onset of apoptosis is smaller than those that form during migration but increases as apoptosis progresses. The enlarged bleb contains substances such as HMGB1 and develops into apoptotic body. Then, how does the change in bleb dynamics mechanistically contribute to the intracellular changes during apoptosis?

I previously analyzed the mechanism of bleb formation during cell migration and identified the involvement of two small GTPases, Rnd3 and RhoA (Fig. 2A). On the one hand, Rnd3 localizes at the plasma membrane only during the expansion phase of bleb dynamics, where it inhibits RhoA through activation of p190-Rho-GAP (16) (Fig. S1B and S1D). On the other hand, RhoA localizes at the plasma membrane only during bleb retraction where it activates ROCK1 (10) (Fig. S1C and S1E). ROCK1 phosphorylates Rnd3, which results in the sequestration of Rnd3 in the cytoplasm via its binding to 14-3-3 protein (17). RhoA also plays a central role in the regulation of the actin cytoskeleton in bleb during retraction. First, during the retraction of membrane blebs, RhoA activates mDia-1, a member of formin family proteins, and induces massive regrowth of actin filaments (18). In addition, ROCK1 activated by RhoA phosphorylates Ezrin and phosphorylated Ezrin promotes the reassembly of the actin cortex by recruiting Eps8 to the plasma membrane (10). Thus, RhoA mediates the rapid recovery of the actin cytoskeleton during the retraction phase. Taken together, I proposed that the reciprocal negative feedback mechanism between Rnd3 and RhoA acts as a master regulator of the reversal of membrane expansion to retraction during blebbing (19) (Fig. 2B).

Therefore, I explored next whether the double negative feedback mechanism between Rnd3 and RhoA is also involved in apoptotic blebbing. I examined the distribution of Rnd3 and RhoA in membrane blebs of apoptosis. I found that the changes in localization of Rnd3 and RhoA during the bleb cycle are common in both apoptotic blebs and blebs formed during cell migration, such that Rnd3 localizes to the plasma membrane in the expanding phase and active RhoA localizes to the plasma membrane in the retraction phase during apoptosis (Figs. 2C and 2D).

RhoA-independent constitutive activation of ROCK1 reduces bleb size

Then, what accounts for the difference in the dynamics of membrane blebs between cell migration and apoptosis? It was demonstrated that ROCK1 is cleaved by activated caspase-3 after induction of apoptosis and becomes constitutively active throughout the course of

apoptosis (6,7). I confirmed that ROCK1 is cleaved at 2 hours after induction of apoptosis by treatment with an anti-Fas antibody (Fig. 3A). Thus, forced activation of ROCK1 by caspase-3 may account for the characteristics of bleb dynamics in the early stage of apoptosis.

I examined whether expression of the constitutively active form of ROCK1 is responsible for reduced bleb size at the early stage of apoptosis by experiments and mathematical simulations. The expression of a constitutive active ROCK1 mutant in non-apoptotic DLD1 cells caused the displacement of Rnd3 from the plasma membrane from the beginning of the expansion phase and accelerated the accumulation of actin filaments (Figs. 3B and 3C). As a result, bleb size and bleb retraction time decreased in DLD1 cells expressing constitutively active ROCK1 relative to control DLD1 cells, and bleb dynamics was instead similar to that in the early stage of apoptosis (Figs. 3D-3G).

Next, I examined the mechanism by which ROCK1 activation caused the reduction of bleb size by mathematical simulation. I constructed a mathematical model of membrane blebs based on the experimentally-identified molecular networks of membrane blebs in freely-moving DLD1 cells, specifically focusing on the double negative feedback loop between Rnd3 and RhoA (Fig. S2A). Parameters in the mathematical simulation were optimized based on measurement values obtained from experimental data (Fig. S2). I simulated the case where ROCK1 is active regardless of the Rnd3-RhoGAP pathway to reflect constitutive ROCK1 activation by caspase-3 during early stage apoptosis. Postulating ROCK1 activity at a consistently high level, promotes actin reassembly, decreases the amount of Rnd3 at the plasma membrane and causes the formation of consistently smaller blebs compared to the control simulation, in agreement with the experimental observation (Fig. 3H).

I next examined whether apoptosis-associated ROCK1 activation increases Rnd3 phosphorylation. It was previously reported that ROCK1-phosphorylated Rnd3 tightly bind to 14-3-3, resulting in the sequestration of Rnd3 in the cytoplasm. Given this background, I found that the amount of Rnd3 bound to 14-3-3 was higher during apoptosis than during cell motility and that the amount of Rnd3 bound to 14-3-3 during apoptosis was

significantly reduced by Y-27632 treatment, indicating that Rnd3 was phosphorylated by ROCK1 during apoptosis (Figs. 4A and 4B). In summary, the feedback loop of Rnd3-RhoA also functions in the bleb dynamics during apoptosis just as with bleb-driven cell migration. However, parallel, RhoA-independent activation of ROCK1 by caspase-3 increased the phosphorylation level of Rnd3 in apoptotic cells relative to migratory cells, resulting in the enhanced removal of Rnd3 from the plasma membrane and the formation of small blebs (Fig. 4C).

Based on these results, I conclude that the decrease in bleb size observed in the early phase of apoptosis is caused by constitutive activation of ROCK1 by caspase-3.

Bleb expansion is triggered by loss of plasma membrane phospholipid asymmetry

Blebs begin to incorporate proteins expelled from the nucleus, such as HMGB-1, at 4 hours after the induction of apoptosis, and their size gradually increases. What accounts for the change in bleb size—and presumably the shift in bias from bleb retraction to bleb expansion—between the early and late stages of apoptosis? I quantified the fluorescence intensities of RFP-Lifeact and GFP-PLCδ-PH in blebs formed during cell migration and during apoptosis and analyzed change in the ratio between the two over time (Figs. 5A-5D). The actin cortex and the level of PtdIns (4,5)P2 in the inner leaflet of plasma membrane decreased as apoptosis progressed.

The exposure of PS to the outer leaflet of the plasma membrane by lipid scramblases during late stage apoptosis contributes to recognition and clearance of apoptotic cells by phagocyte. Recently, it was revealed that activation of the lipid scramblase Xkr8 by caspase-3 is responsible for PS translocation during apoptosis (20). The activation of lipid scramblase causes the exposure not only of PS but also other phospholipid species present in the inner leaflet of the plasma membrane. Phosphatidylinositol 4,5-bisphosphate (PtdIns(4,5)P2) is an important component of the plasma membrane inner leaflet where it is essential for the polymerization of actin cytoskeleton and the proteins such as Ezrin that link the plasma membrane to the actin

cytoskeleton (21). Therefore, I considered the possibility that the decrease in actin cytoskeleton observed in the late stage of apoptosis may be caused by the decrease in PtdIns(4,5)P2 at the inner leaflet of the plasma membrane. Actually, live imaging of DLD1 cells expressing GFP-PLCδ-PH, which is known to bind to specifically (22), indicated that the amount of PtdIns(4,5)P2 at the inner leaflet of plasma membrane was significantly reduced in the late stage of apoptosis as compared to the early stage (Figs. 5C and 5D).

I stained apoptotic DLD1 cells with the purified PtdIns(4,5)P2 probe GFP-PLCδ-PH to examine whether PtdIns(4,5)P2 is translocated to the outer leaflet of the plasma membrane during apoptosis. Phosphatidylserine and PtdIns(4,5)P2 are exposed at the outer leaflet of the plasma membrane in apoptotic cells. Accordingly, cells undergoing apoptosis, but not migratory cells, were prominently stained by Annexin-V and GFP-tagged PLCδ-PH domain protein and Annexin-V, specific probes for PS and PtdIns(4,5)P2, respectively (Fig. 5E).

I next examined whether artificially decreasing PtdIns(4,5)P2 from the inner leaflet of plasma membrane could increase bleb size similar to late stage apoptosis. I over-expressed a constitutively-active mutant of Xkr8 (23) in freely moving DLD1 cells and examined the changes of bleb dynamics (Figs. 5F-5K). In cells expressing the constitutively active form of Xkr8, the size of bleb was significantly enlarged (Fig. 5I). I next examined whether activation of Xkr-8 by caspase-3 cleavage can expose PtdIns(4,5)P2 to the outer leaflet of the plasma membrane and decrease PtdIns(4,5)P2 in the inner leaflet of the plasma membrane. Cells over-expressing the dominant active form of Xkr-8 were broadly stained with GFP-PLCδ-PH, indicating that PtdIns(4,5)P2 is exposed to the outer leaflet of the plasma membrane in these cells (Fig. 5L). Next, I established DLD1 cells stably expressing GFP-PLCδ-PH to visualize PtdIns(4,5)P2 in the inner leaflet of the plasma membrane. In these cells, expression of dominant active Xkr-8 reduced the signal derived from GFP-PLCδ-PH, indicating that PtdIns(4,5)P2 was reduced in the inner leaflet of the plasma membrane by expression of dominant active Xkr-8 (Figs. 5M and 5N). Based on these findings, I concluded that at the later stage of apoptosis, scrambling of phospholipids lead to the reduction of amount of PtdIns(4,5)P2 present in the inner leaflet

of plasma membrane, which reduces actin polymerization and the plasma membrane cross-linking activity of Ezrin during retracting phase, resulting in the formation of larger blebs. On the other hand, it was reported that actin molecules are degraded by caspases during apoptosis (24). Taken together, the reduction of PtdIns(4,5)P2 in the inner leaflet of plasma membrane by scramblase activation and the degradation of actin by caspases cooperatively contribute to the destruction of the actin cortex and the enlargement of blebs during late stage apoptosis.

Discussion

In this study, I analyzed the molecular mechanism of changes in bleb dynamics during apoptosis. I showed that Rnd3 and RhoA are localized to the apoptotic bleb, indicating that the double negative feedback loop between Rnd3 and RhoA is a core machinery of bleb cycle in the apoptosis similar to the case of cell migration. Furthermore, I demonstrated that the changes of apoptotic blebs in the dynamics of bleb expansion and retraction is caused by constitutive activation of ROCK1 and Xkr8 by caspase-3.

In the apoptosis, membrane blebs function as concentration sites for phagocytic markers and help apoptotic cells to be detected and phagocytosed by phagocytes and/or neighboring cells (25). By packing the cytoplasmic contents into apoptotic bodies, it prevents the dissemination of intracellular degradation products that can become autoantigens and avoids unnecessary immune responses (26, 27). Furthermore, interleukin-1α or DAMPs such as HMGB1 in the apoptotic body are recently reported to modulate immune cell responses (28, 29, 30). Thus, the importance of apoptotic blebs has become widely recognized (8).

Apoptotic bleb contains substances necessary for communication with surrounding cells, not just cellular debris or by-products of apoptosis. I found that HMGB1 translocation to the cytoplasm of blebs was impaired in apoptotic cells in which bleb formation is suppressed by the treatment with Y-27632. I demonstrated that ROCK1 activation by caspase-3 was required for the induction of small blebs at the early phase of apoptosis and large bleb enough to contain substances such as HMGB1 was formed by the loss of asymmetric distribution of PtdIns(4,5)P2 during maturation of apoptotic body (Fig. 6). Future studies need to clarify how changes in the cytoplasm and changes in membrane dynamics are coordinated in order to form functional apoptotic bleb containing various immune-modulating substances.

Materials and Methods

Reagents

DLD1 cells were purchased from ATCC. DLD1 cells were grown in DMEM supplemented with 10% (vol/vol) FCS. The following primary antibodies were used for immunoblotting: mouse anti-ROCK1 antibody mAb (Abcam), mouse anti–α-tubulin mAb (Sigma), rabbit anti-Lamin A/C antibody pAb (Cell Signaling Technology). cDNAs encoding full length human Rnd3, human Anillin C terminus, human Xkr8ΔC, human Lamin A and human 14-3-3βwere amplified by RT-PCR, fused to the sequence encoding enhanced GFP or FLAG tag, and ligated into the pCAGGS-neo vector. pEGFP-CytochromeC, and pcDNA3-FlipGFP (Casp3 cleavage seq) T2A mCherry were obtained from Addgene (No. 41181 and No. 124428).

Live Imaging

All fluorescence imaging was performed using a 63× oil-immersion objective on an inverted microscope (LSM700; Carl Zeiss Micro Imaging) interfaced to a laser-scanning confocal microscope equipped with a heating stage heated to 37 ℃. Phosphatidylserine exposed on the outer leaflet of the plasma membrane is stained by using Annexin V-Cy3 Apoptosis Detection Kit (Biovision). Images were captured on a device camera and acquired on a PC using ZEN2012 software (LSM700; Carl Zeiss MicroImaging). Images were acquired at 488 nm for GFP-tagged proteins or at 555 nm for RFP-tagged proteins. Each imaging video frame is a 8-bit grayscale image, and the frame interval is indicated in the figure legends. The movie captures a single cell.

Immunoblotting

Cells were treated with anti-Fas antibody (SY-001) purchased from MBL (Nagoya, Japan) (250 ng /mL) and cycloheximide purchased from Sigma (St Louis Mo) (10 mg/mL) to induce apoptosis. To inhibit ROCK or pan-caspase activity during apoptosis, cells were also treated with ROCK inhibitor Y-27632 (10μM) or caspase inhibitor Z-VAD-FMK (50μM) purchased from MBL (Nagoya, Japan). Cells were washed with PBS and dissolved in SDS sample buffer. Aliquots of the cell lysate were immunoblotted with anti-ROCK1 antibody, anti-Lamin A/C antibody and anti-α-tubulin antibody. The signal intensity was quantified by using imageJ.

Immunoprecipitation

Cells were treated with 250 ng /mL anti-Fas antibody (SY-001) purchased from MBL (Nagoya, Japan) and 10 mg/mL cycloheximide purchased from Sigma (St Louis Mo) to induce apoptosis. To inhibit ROCK or pan-caspase activity during apoptosis, cells were also treated with 10μM Y-27632 or 50μM Z-VAD-FMK purchased from MBL (Nagoya, Japan). Cells were washed with PBS and lysed with IP buffer (20 mM Tris-HCl [pH 7.5], 150 mM NaCl, 1% Triton X-100, and protease inhibitors). Lysates were incubated with 10μl of anti-DYKDDDDK mAb beads (Wako Pure Chemical Industries) for 2h. Beads were washed with IP buffer and bound proteins were eluted in SDS sample buffer. Aliquots of the lysate and eluate were immunoblotted with anti-FLAG antibody and anti-GFP antibody. The signal intensity was quantified by using imageJ.

Visualization and quantitative analysis of membrane bleb dynamics

I previously described the method of image analysis for visualization of membrane bleb dynamics in detail (10). A tricolor map visualizes the membrane bleb dynamics more directly (Fig. S1). It is a (θ, t)-visualization and the angle θ corresponds to the cell contour

point in the direction θ from the center of the gravity of the cell. If the contour point lies on an expanding (retracting) bleb at t, the pixel (θ, t) is printed in red (blue) in the tricolor map. Otherwise, that is, if the contour point is rather stationary, the pixel is printed in white. The intensity of fluorescent protein was quantified using Fiji / ImageJ.

Figures

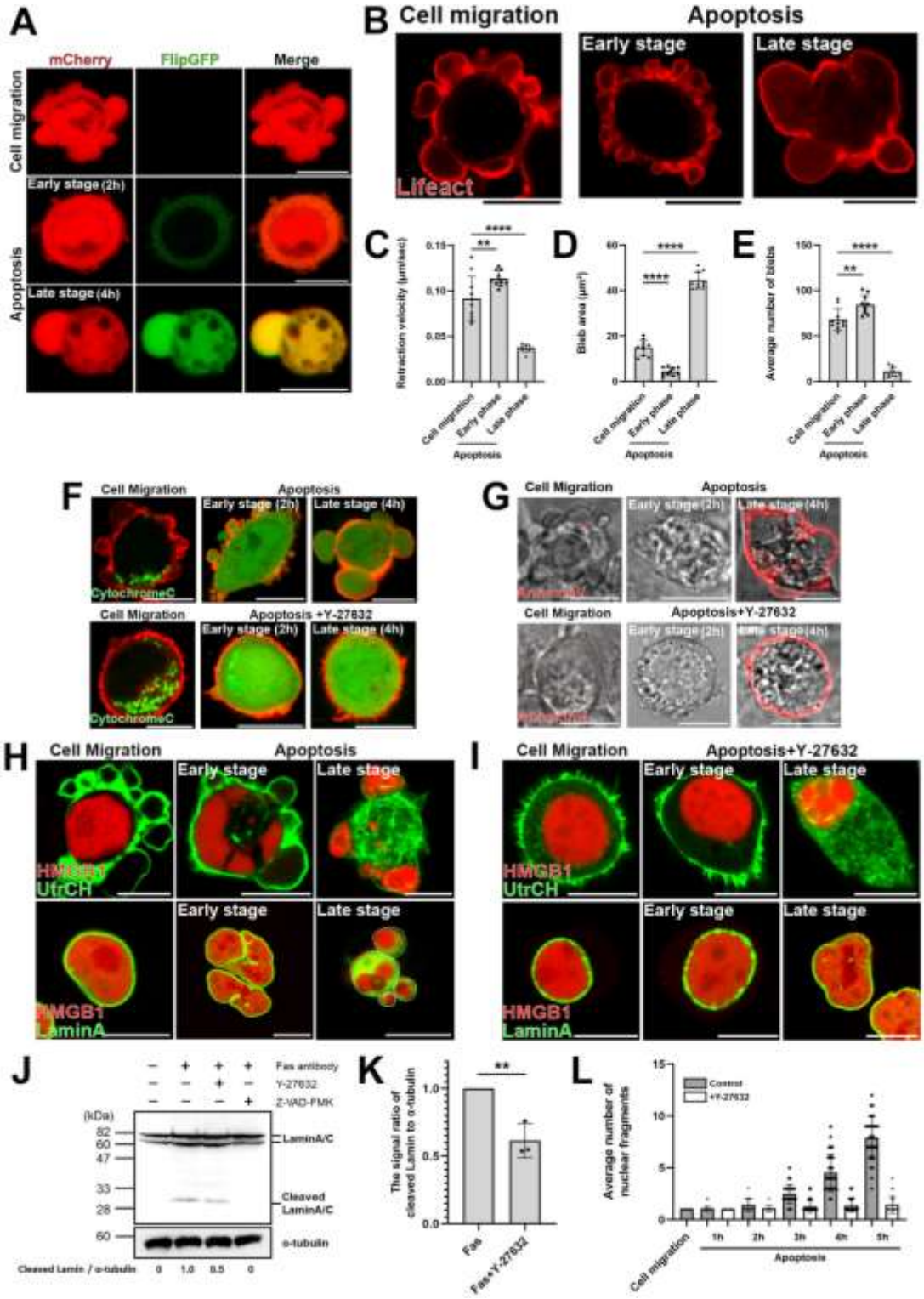
A
mCherry
FlipGFP
Merge
Cell migration
Early stage (2h)
Late stage (4h)
Apoptosis
B
Cell migration
Apoptosis
Early stage
Late stage
Lifeact
C
Retraction velocity (μm/sec)
Cell migration
Early phase
Late phase
Apoptosis
D
Bleb area (μm²)
E
Average number of blebs
F
Cell Migration
Apoptosis
Early stage (2h)
Late stage (4h)
CytochromeC
Apoptosis +Y-27632
G
Apoptosis+Y-27632
H
HMGB1
UtrCH
LaminA
I
J
Fas antibody
Y-27632
Z-VAD-FMK
(kDa)
82
60
47
33
28
50
LaminA/C
Cleaved LaminA/C
α-tubulin
Cleaved Lamin / α-tubulin
K
The signal ratio of cleaved Lamin to α-tubulin
Fas
Fas+Y-27632
L
Average number of nuclear fragments
Control
+Y-27632
1h
2h
3h
4h
5h

Figure 1. The dynamic behavior of membrane blebs changes with the progression of apoptosis

(A) Migratory blebs and apoptotic blebs of DLD1 cells stably expressing FlipGFP(casp3)-T2A-mCherry, a GFP-based fluorogenic caspase-3 reporter. When DLD1 cells were seeded on Type I Collagen gel, they actively formed blebs and moved around freely (upper). DLD1 cells were treated with 250 ng /mL anti-Fas antibody and 10 mg/mL cycloheximide for 2 hours (Early stage) or 4 hours (Late stage) to induce apoptosis (Lower). Results shown are representative of three independent experiments. Scale bar, 10 μm.

(B) DLD1 cells were transfected with Lifeact-RFP. DLD1 cells actively formed blebs and moved around freely (left). DLD1 cells were treated with 250 ng /mL anti-Fas antibody and 10 mg/mL cycloheximide for 2 hours (Early stage) or 4 hours (Late stage) to induce apoptosis (Right). Results shown are representative of five independent experiments. Scale bar, 10 μm.

(C) The retraction velocities of membrane blebs in freely-moving DLD1 cells and apoptotic DLD1 cells were quantified. The speed of the retraction phase of membrane blebs of apoptotic cells in the late stage was slower than that in early stage. Error bars indicate the standard deviation (SD) calculated based on the values from N=10 independent blebs. **P < 0.01, ****P < 0.0001 (One-way ANOVA).

(D) The sizes of membrane blebs in freely-moving DLD1 cells and apoptotic DLD1 cells were quantified. The size of membrane blebs of apoptotic cells in the late stage was significantly larger than that in early stage. Error bars are SD of N=10 independent blebs. ****P < 0.0001 (One-way ANOVA).

(E) The frequencies of membrane blebs in freely-moving DLD1 cells and apoptotic DLD1 cells during 10 min were quantified. The number of blebs formed during 10 min in apoptotic cells in the late stage was significantly fewer than that in early stage. Error bars are SD of N=10 independent blebs. **P < 0.01, ****P < 0.0001 (One-way ANOVA).

(F) (Upper panel) Membrane blebbing of DLD1 cells transfected with Cytochrome C-GFP and Lifeact–RFP from the early stage to the late stage of apoptosis. Cells were treated with 250 ng /mL anti-Fas antibody and 10 mg/mL cycloheximide for 2 hours (Early stage) and 4 hours (Late stage). (Lower panel) Membrane blebbing of DLD1 cells transfected with Cytochrome C-GFP and Lifeact–RFP from the early stage to the late stage of apoptosis under ROCK inhibition. Cells were treated with 250 ng /mL anti-Fas antibody, 10 mg/mL cycloheximide and 10 μM Y-27632 for 2 hours (Early stage) and 4 hours (Late stage). Results shown are representative of three independent experiments. Scale bar, 10 μm.

(G) (Upper panel) Membrane blebbing of DLD1 cells stained with AnnexinV-Cy3 from the early stage to the late stage of apoptosis. Cells were treated with 250 ng /mL anti-Fas antibody and 10 mg/mL cycloheximide for 2 hours (Early stage) and 4 hours (Late stage). (Lower panel) Membrane blebbing of DLD1 cells stained with AnnexinV-Cy3 from the early stage to the late stage of apoptosis under ROCK inhibition. Cells were treated with 250 ng /mL anti-Fas antibody, 10 mg/mL cycloheximide and 10 μM Y-27632 for 2 hours (Early stage) and 4 hours (Late stage). Results shown are representative of three independent experiments. Scale bar, 10 μm.

(H) (Upper panel) Membrane blebbing of DLD1 cells transfected with the calponin homology domain of utrophin (UtrCH)-GFP, a filamentous actin marker, and HMGB1-mScarlet from the early stage to the late stage of apoptosis. Cells were treated with 250 ng /mL anti-Fas antibody and 10 mg/mL cycloheximide for 2 hours (Early stage) and 4 hours (Late stage). (Lower panel) Membrane blebbing of DLD1 cells transfected with LaminA–GFP and HMGB1-mScarlet from the early stage to the late stage of apoptosis. Cells were treated with 250 ng /mL anti-Fas antibody and 10 mg/mL cycloheximide for 2 hours (Early stage) and 4 hours (Late stage). White broken lines indicate margin of large blebs formed during the late phase of apoptosis. Results shown are representative of three independent experiments. Scale bar, 10 μm.

(I) (Upper panel) Membrane blebbing of DLD1 cells transfected with UtrCH-GFP and HMGB1-mScarlet from the early stage to the late stage of apoptosis under ROCK

inhibition. Cells were treated with 250 ng /mL anti-Fas antibody, 10 mg/mL cycloheximide and 10 μM Y-27632 for 2 hours (Early stage) and 4 hours (Late stage). Scale bar, 10 μm. (Lower panel) Membrane blebbing of DLD1 cells transfected with LaminA-GFP and HMGB1-mScarlet from the early stage to the late stage of apoptosis under ROCK inhibition. Cells were treated with 250 ng /mL anti-Fas antibody, 10 mg/mL cycloheximide and 10 μM Y-27632 for 2 hours (Early stage) and 4 hours (Late stage). Results shown are representative of three independent experiments. Scale bar, 10 μm.

(J) DLD1 cells were left untreated or treated with 250 ng /mL anti-Fas antibody and 10 mg/mL cycloheximide for 4 h to induce apoptosis, either in the absence or presence of 10μM Y-27632 or 50μM Z-VAD-FMK as indicated. Lysates were run on 10% SDS-PAGE and immunoblotted with anti-LaminA/C and α-tubulin antibodies. Cleaved LaminA/C and α-tubulin signals were quantified by densitometry to derive the ratio of cleaved LaminA/C to α-tubulin. The signal ratio of DLD1 cells treated with anti-Fas antibody and cycloheximide only (Lane2) was set to 1. Results shown are representative of three independent experiments.

(K) The quantified means from N = 3 independent experiments of the signal ratio of cleaved LaminA/C to α-tubulin shown in (J). Error bars indicate the SD. **P < 0.01 (Student's t test).

(L) Quantitative analysis of changes in the number of nuclear fragments labeled with HMGB1-mScarlet from the early stage to the late stage of apoptosis. Cells were treated with 250 ng /mL anti-Fas antibody and 10 mg/mL cycloheximide with or without 10 μM Y-27632 for 5 hours. The number of HMGB1-mScarlet fragments were counted every hour. The SD was calculated based on the values from N=30 independent cells.

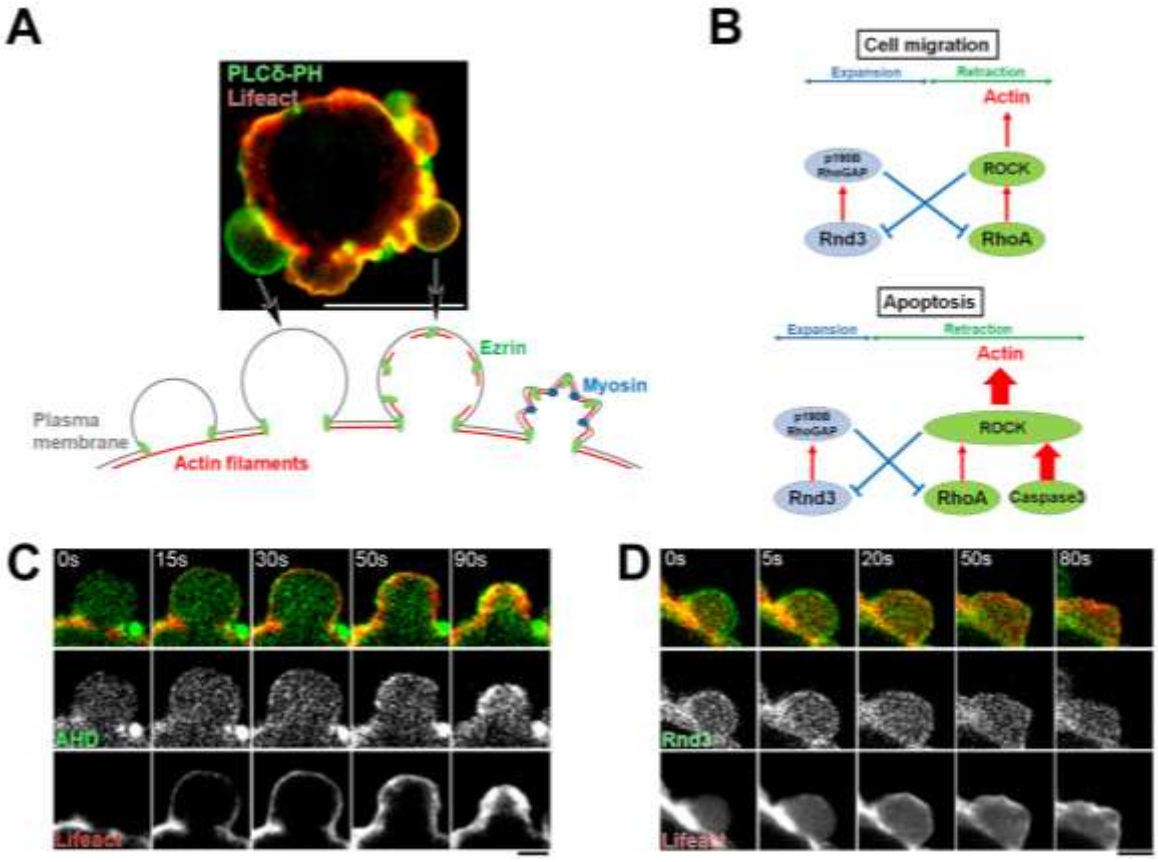
A
PLCδ-PH
Lifeact
Ezrin
Myosin
Plasma membrane
Actin filaments
B
Cell migration
Expansion
Retraction
Actin
p190B RhoGAP
ROCK
Rnd3
RhoA
Apoptosis
Expansion
Retraction
Actin
p190B RhoGAP
ROCK
Rnd3
RhoA
Caspase3
C
0s
15s
30s
50s
90s
AHD
Lifeact
D
0s
5s
20s
50s
80s
Rnd3
Lifeact

Figure2. Dynamics of membrane bleb during early stage apoptosis

(A) Membrane blebbing of DLD1 cells transfected with Lifeact–RFP and GFP-tagged PLCδ-PH domain. Arrows indicate representative examples of the expanding bleb and the retracting bleb. Scale bar, 10 μm.

(B) Models describing the regulation of actin cortex by the interplay between Rnd3 and RhoA during membrane blebbing of migrating cells and apoptotic cells.

(C) Membrane blebbing of DLD1 cells transfected with Lifeact–RFP and Anillin homology domain (AHD)-GFP, a biosensor for the detection of active RhoA, and treated with 250 ng /mL anti-Fas antibody and 10 mg/mL cycloheximide for 2 hours. AHD-GFP was recruited to retracting membrane blebs where reassembly of the actin cortex occurred. Results shown are representative of three independent experiments. Scale bar, 2 μm.

(D) Membrane blebbing of DLD1 cells transfected with Lifeact–RFP and Rnd3-GFP and treated with 250 ng /mL anti-Fas antibody and 10 mg/mL cycloheximide for 2 hours. Rnd3 was recruited to expanding membrane blebs; however, this membrane localization was gradually lost upon the initiation of retraction of bleb (t = 20 sec). Results shown are representative of three independent experiments. Scale bar, 2 μm.

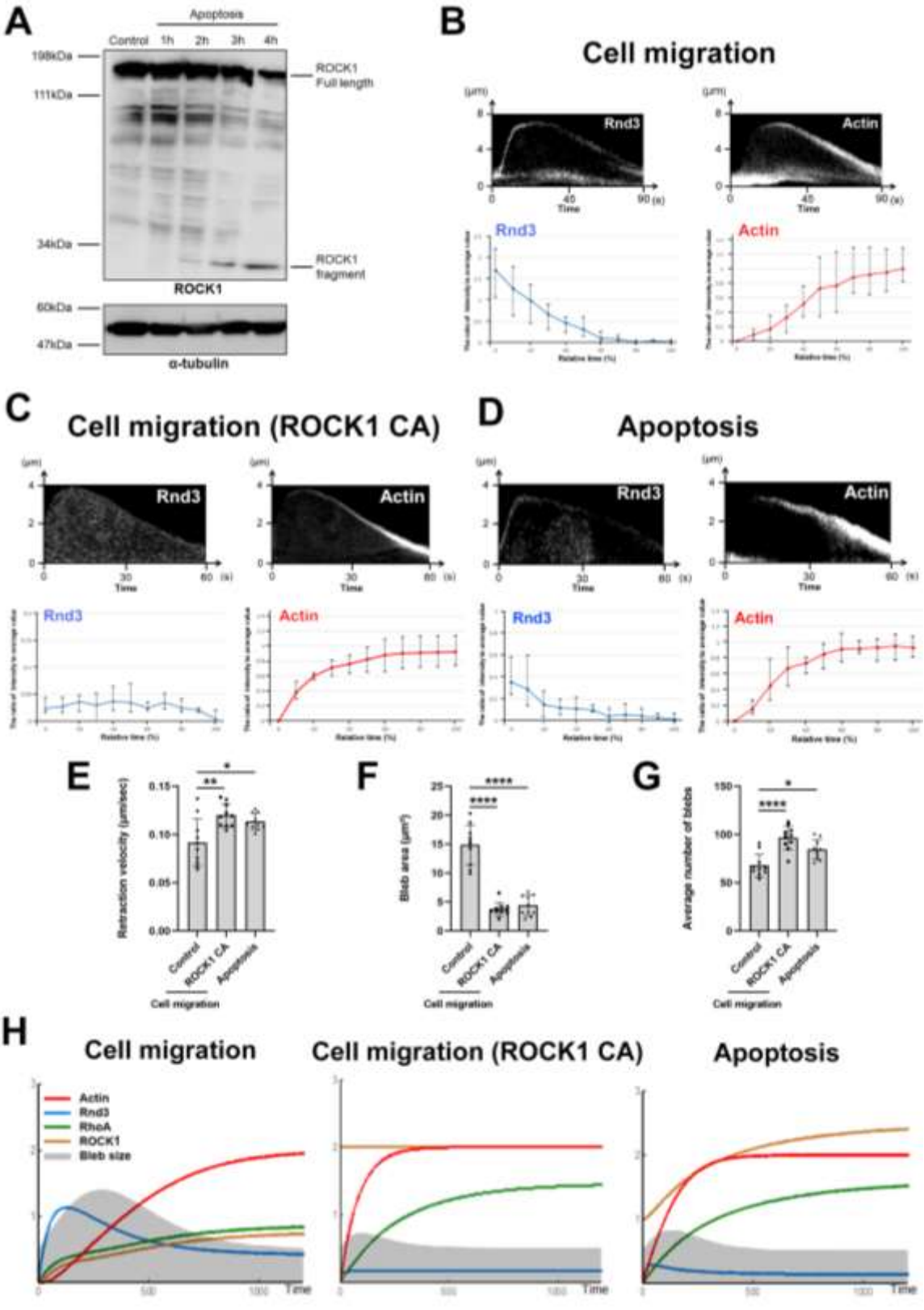
A
Apoptosis
Control
1h
2h
3h
4h
198kDa
111kDa
34kDa
ROCK1
Full length
ROCK1
fragment
ROCK1
60kDa
47kDa
α-tubulin
B
Cell migration
Rnd3
Actin
Time
Relative time (%)
C
Cell migration (ROCK1 CA)
D
Apoptosis
E
Retraction velocity (μm/sec)
F
Blob area (μm²)
G
Average number of blebs
Control
ROCK1 CA
Apoptosis
Cell migration
H
Cell migration
Cell migration (ROCK1 CA)
Apoptosis
Actin
Rnd3
RhoA
ROCK1
Bleb size
Time

Figure3. The mathematical simulation of bleb dynamics in the early phase of apoptosis

(A) Total cell lysates of DLD1 cells treated with 250 ng /mL anti-Fas antibody and 10 mg/mL cycloheximide for 1, 2, 3, and 4 hours were resolved by SDS-PAGE and immunoblotted with anti-ROCK1 and α-tubulin antibodies. The 30-kDa band corresponding to the cleaved ROCK1 fragment was increased with the progression of apoptosis. Results shown are representative of three independent experiments.

(B) (Upper panel) Kymographs showing the localization of Rnd3 (left) and actin filaments (right) during bleb retraction in migrating DLD1 cells (Cell migration). Bleb extension is shown on the vertical axis, and time (sec) is shown on the horizontal axis. Results shown are representative of five independent experiments. Rnd3 was recruited to the plasma membrane of expanding membrane blebs where reassembly of the actin cortex did not occur. (Lower panel) Quantitative analysis of changes in fluorescence intensity of GFP-Rnd3 or RFP-Lifeact in membrane blebs. For each of five independent cells, a single bleb was selected from a single cell, and the fluorescence intensity during bleb retraction was measured in a total of 5 independent blebs. The value obtained by subtracting the minimum fluorescence intensity (background) from the fluorescence intensity at each time point was divided by the average fluorescence intensity value to obtain the relative fluorescence intensity value at each time.

(C) (Upper panel) Kymographs showing the localization of Rnd3 (left) and actin filaments (right) during bleb retraction in freely-moving DLD1 cells expressing ROCK1ΔC (constitutive active: CA). Bleb extension is shown on the vertical axis, and time (sec) is shown on the horizontal axis. Results shown are representative of five independent experiments. The localization of Rnd3 at the plasma membrane was impaired in DLD1 cells expressing ROCK1 CA. (Lower panel) Quantitative analysis of changes in fluorescence intensity of GFP-Rnd3 or RFP-Lifeact in membrane blebs of freely-moving DLD1 cells expressing ROCK1 CA. For each of five independent cells, a single bleb was selected from a single cell, and the fluorescence intensity during bleb retraction was

measured in a total of 5 independent blebs. The value obtained by subtracting the minimum fluorescence intensity (background) from the fluorescence intensity at each time point was divided by the average fluorescence intensity value to obtain the relative fluorescence intensity value at each time.

(D) (Upper panel) Kymographs showing the localization of Rnd3 (left) and actin filaments (right) during bleb retraction in early-phase apoptotic DLD1 cells during the early stage of apoptosis. Bleb extension is shown on the vertical axis, and time (sec) is shown on the horizontal axis. Results shown are representative of five independent experiments. The localization of Rnd3 at the plasma membrane was impaired in DLD1 cells in the early stage of apoptosis. (Lower panel) Quantitative analysis of changes in fluorescence intensity of GFP-Rnd3 or RFP-Lifeact in membrane blebs during the early stage of apoptosis. For each of five independent cells, a single bleb was selected from a single cell, and the fluorescence intensity during bleb retraction was measured in a total of 5 independent blebs. The value obtained by subtracting the minimum fluorescence intensity (background) from the fluorescence intensity at each time point was divided by the average fluorescence intensity value to obtain the relative fluorescence intensity value at each time.

(E) The retraction velocities of membrane blebs in control DLD1 cells, ROCK1 CA expressing DLD1 cells and early-phase apoptotic DLD1 cells were quantified. The SD was calculated based on the values from N=10 independent blebs. *$P < 0.05$, **$P < 0.01$ (One-way ANOVA).

(F) The sizes of membrane blebs in control DLD1 cells, ROCK1 CA overexpressing DLD1 cells and early-phase apoptotic DLD1 cells were quantified. The SD was calculated based on the values from N=10 independent blebs. ****$P < 0.0001$ (One-way ANOVA).

(G) The frequencies of membrane blebs in control DLD1 cells, ROCK1 CA expressing DLD1 cells and early-phase apoptotic DLD1 cells during 10 min were quantified. The SD was calculated based on the values from N=10 independent cells. *$P < 0.05$, ****$P < 0.0001$ (One-way ANOVA).

(H) Results of mathematical simulation of bleb dynamics in migrating DLD1 cell (left), ROCK1 CA expressing cell (middle) and early-phase apoptotic cell (right). For the details of mathematical simulations, please see Fig. S2. The figures show the results of mathematical simulations for the cycle of expansion and retraction of bleb in each condition. The gray shape shows the change in size of the bleb over time. The red line shows the amount of actin in the plasma membrane, the blue line shows the amount of Rnd3 in the plasma membrane, the green line shows the amount of activated RhoA in the plasma membrane, and the yellow line shows the amount of activated ROCK1 in the plasma membrane. The unit of time axis (horizontal axis) and vertical axis is arbitrary.

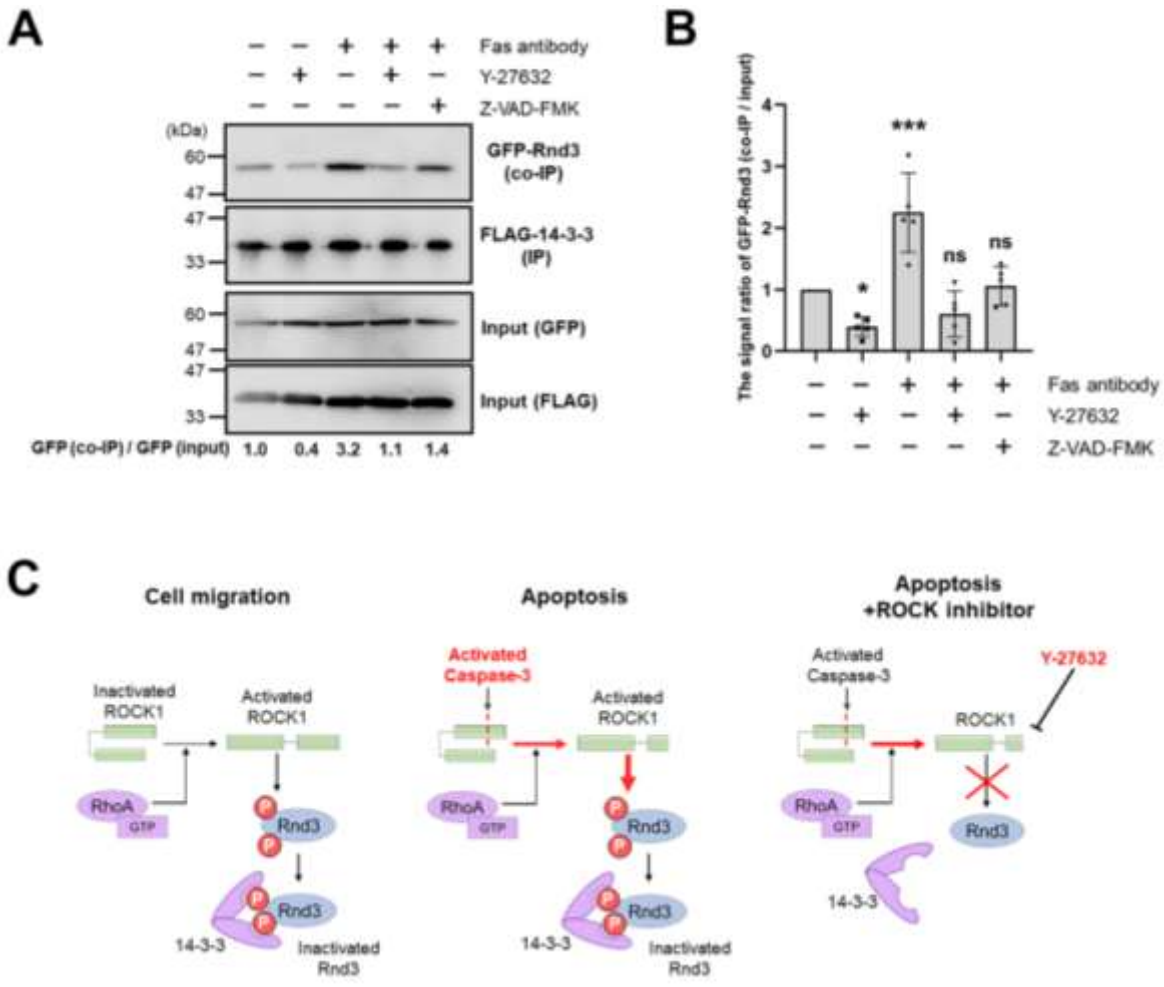
A
Fas antibody
Y-27632
Z-VAD-FMK
(kDa)
60
47
GFP-Rnd3
(co-IP)
47
33
FLAG-14-3-3
(IP)
60
47
Input (GFP)
47
33
Input (FLAG)
GFP (co-IP) / GFP (input) 1.0 0.4 3.2 1.1 1.4
B
The signal ratio of GFP-Rnd3 (co-IP / input)
*
***
ns
ns
Fas antibody
Y-27632
Z-VAD-FMK
C
Cell migration
Apoptosis
Apoptosis
+ROCK inhibitor
Inactivated
ROCK1
Activated
ROCK1
RhoA
GTP
Rnd3
14-3-3
Inactivated
Rnd3
Activated
Caspase-3
Y-27632

Figure4. ROCK1 regulates Rnd3 interaction with 14-3-3 during apoptosis

(A) DLD1 cells co-expressing FLAG-14-3-3β and GFP-Rnd3 were treated with 250 ng /mL anti-Fas antibody and 10 mg/mL cycloheximide for 3 hours to induce apoptosis in conjunction with either 10 μM Y-27632 or 50 μM Z-VAD-FMK. Lysates were prepared and immunoprecipitated with anti-FLAG antibody-conjugated beads and the precipitates were probed with anti-GFP or anti-FLAG antibodies. GFP-Rnd3 (co-IP) and GFP-Rnd3 (input) signals were quantified by densitometry to obtain the ratio co-IP to input. The signal ratio of control cells was set to 1. Results shown are representative of five independent experiments.

(B) The means of N = 5 independent experiments represented by (A) are shown with the SD. *P < 0.05, ***P < 0.001 (One-way ANOVA).

(C)A model describing the regulation of Rnd3 activation by ROCK1 and 14-3-3 during apoptosis.

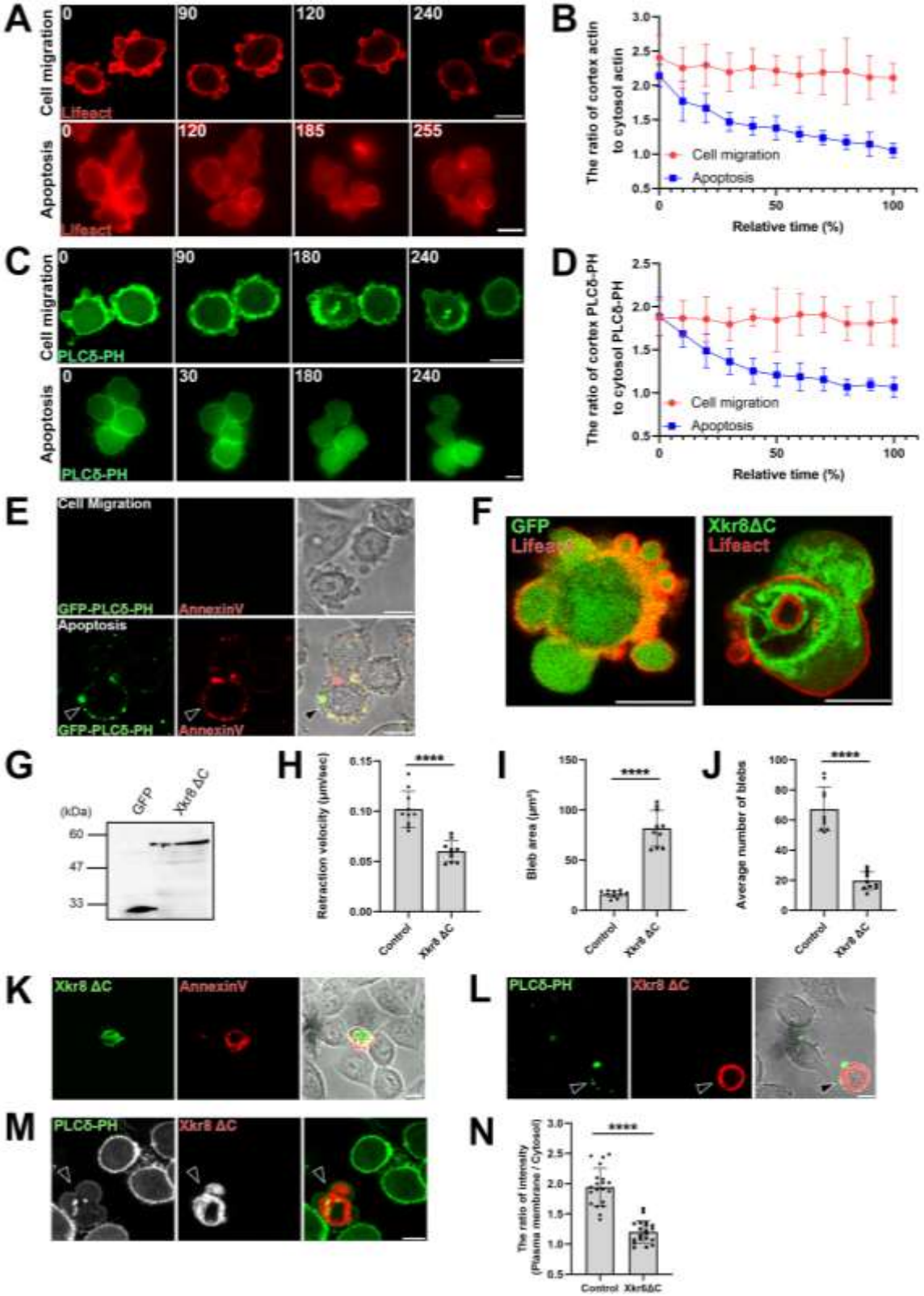
A
Cell migration
Apoptosis
Lifeact
0
90
120
240
185
255
B
The ratio of cortex actin to cytosol actin
Cell migration
Apoptosis
Relative time (%)
C
PLCδ-PH
30
180
D
The ratio of cortex PLCδ-PH to cytosol PLCδ-PH
E
Cell Migration
GFP-PLCδ-PH
AnnexinV
Apoptosis
F
GFP
Lifeact
Xkr8ΔC
G
(kDa)
GFP
Xkr8 ΔC
60
47
33
H
Retraction velocity (μm/sec)
****
Control
Xkr8 ΔC
I
Bleb area (μm²)
J
Average number of blebs
K
Xkr8 ΔC
AnnexinV
L
PLCδ-PH
M
N
The ratio of intensity (Plasma membrane / Cytosol)
Control
Xkr8ΔC

Figure5. Bleb expansion is triggered by loss of plasma membrane phospholipid asymmetry

(A) and (C) Membrane blebbing of migrating (upper panels) and apoptotic (lower panels) DLD1 cells expressing either Lifeact–RFP (A) or PLCδ-PH-GFP (C). Apoptosis was induced by simultaneous treatment with 250 ng /mL anti-Fas antibody and 10 mg/mL cycloheximide for 3 hours. Times indicated are relative to an arbitrary starting point for migratory cells and to the first image after treatment for apoptotic cells (min). Results shown are representative of five independent experiments. Scale bar, 10 μm.

(B) and (D) Quantification of experiments depicted in (A) and (C). Fluorescence intensities of either Lifeact-RFP (B) or PLCδ-PH-GFP (D) were measured at the cell cortex and the cytosol and their ratio were plotted against time. The SD was calculated based on the values from N = 5 independent experiments.

(E) PtdIns(4,5)P2 and PS exposure to the outer leaflet of the plasma membrane during apoptosis. Cells were treated with 250 ng /mL anti-Fas antibody and 10 mg/mL cycloheximide for 4 hours. Migrating and late-phase apoptotic cells were stained with purified GFP-tagged PLCδ-PH protein and AnnexinV-Cy3. Arrowhead shows the apoptotic cell stained with PLCδ-PH and AnnexinV. Of note, the attachment of lipid binding proteins such as PLCδ-PH or Annexin V to the outer leaflet of plasma membranes inhibits bleb expansion. Therefore, the morphology of blebs of cells stained with these proteins are different from that of untreated cells. Result shown is representative of three independent experiments. Scale bar, 10 μm.

(F) Membrane blebbing of DLD1 cells transfected with GFP tag only and Lifeact- RFP (left) and membrane blebbing of DLD1 cells transfected with GFP-tagged Xkr8ΔC, a constitutively active form of Xkr8, and Lifeact-RFP (right). Result shown is representative of three independent experiments. Scale bar, 10 μm.

(G) Total cell lysates of DLD1 cells expressing GFP tag only and GFP-tagged Xkr8ΔC separated by SDS-PAGE and immunoblotted with an anti-GFP mAb.

(H) The retraction velocities of membrane blebs in freely-moving DLD1 cells (Control) and freely-moving DLD1 cells expressing Xkr8ΔC-GFP were quantified. The SD was calculated based on the values from N=10 independent blebs. ****P < 0.0001 (Student's t test). Expression of Xkr8ΔC-GFP led to the reduction in the speed of the retraction phase of membrane blebs.

(I) The sizes of membrane blebs in freely-moving DLD1 cells (Control) and freely-moving DLD1 cells expressing Xkr8ΔC-GFP were quantified. The SD was calculated based on the values from N=10 independent blebs. ****P < 0.0001 (Student's t test). Expression of Xkr8ΔC-GFP led to the enlargement of bleb size.

(J) The frequencies of membrane blebs in freely-moving DLD1 cells (Control) and freely-moving DLD1 cells expressing Xkr8ΔC-GFP during 10 min were quantified. The SD was calculated based on the values from N=10 independent cells. ****P < 0.0001 (Student's t test).

(K) PS exposure in Xkr8ΔC expressing DLD1 cell. Cells were stained with AnnexinV-Cy3. Result shown is representative of three independent experiments. Scale bar, 10 μm.

(L) DLD1 cells expressing RFP-tagged Xkr8ΔC were stained with purified GFP-tagged PLCδ-PH protein to detect PtdIns(4,5)P2 exposure to the outer leaflet of the plasma membrane (arrowheads). Result shown is representative of five independent experiments. Scale bar, 10 μm.

(M) PtdIns(4,5)P2 localization at the inner leaflet of the plasma membrane was observed by stably expressing PLCδ-PH-GFP in DLD1 cells. Arrowhead indicates the Xkr8ΔC-RFP-co-expressing cell. Result shown is representative of five independent experiments. Scale bar, 10 μm.

(N) The fluorescence intensity of the PLCδ-PH-GFP (inner leaflet) signal was quantified in wild-type DLD1 cells and Xkr8ΔC-RFP-expressing DLD1 cells. The SD was calculated based on the values from N=20 independent cells. ****P < 0.0001 (Student's t test).

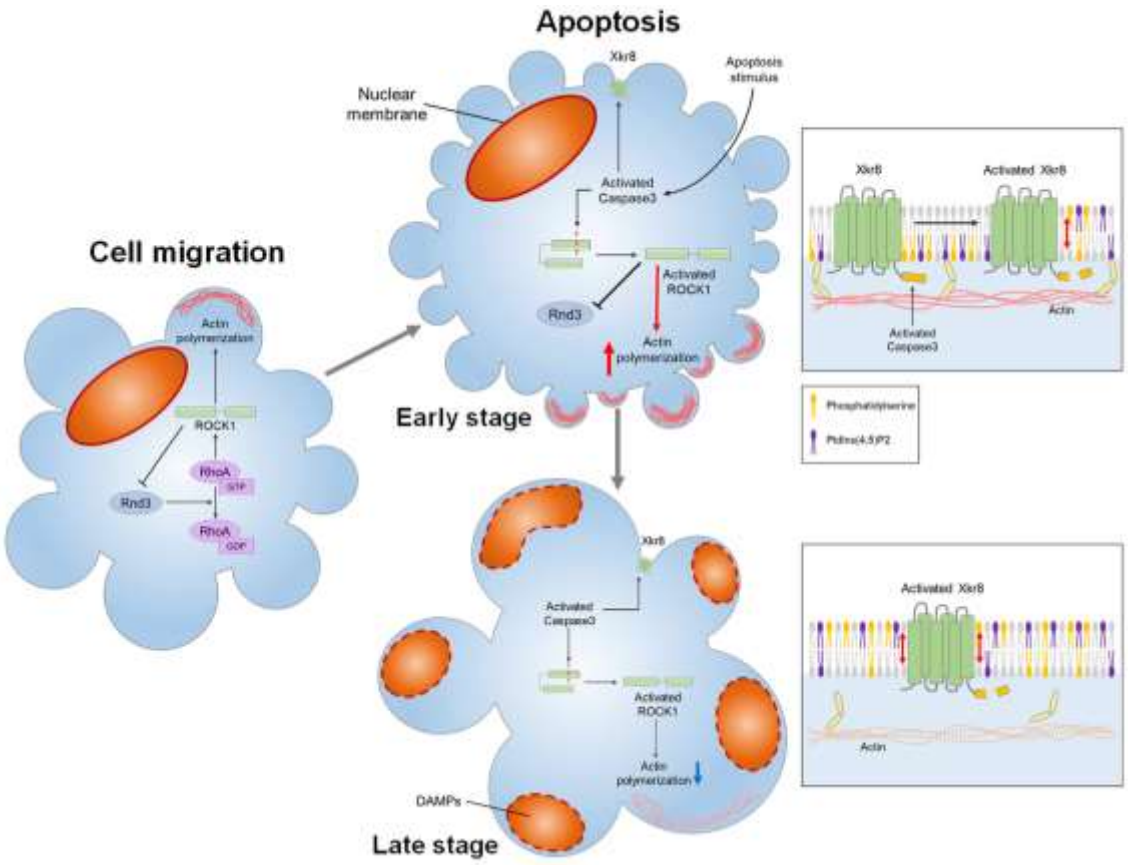
Apoptosis
Xkr8
Apoptosis stimulus
Nuclear membrane
Activated Caspase3
Activated ROCK1
Rnd3
Actin polymerization
Early stage
Cell migration
Actin polymerization
ROCK1
RhoA GTP
Rnd3
RhoA GDP
Xkr8
Activated Caspase3
Activated ROCK1
Actin polymerization
DAMPs
Late stage
Xkr8
Activated Xkr8
Activated Caspase3
Actin
Activated Xkr8
Actin
Phosphatidylserine
PtdIns(4,5)P2

Figure6. The size of apoptotic blebs changes with the progression of apoptosis

In freely-moving cells, bleb cycle is regulated by the double negative feedback loop between Rnd3-p190RhoGAP and RhoA-ROCK1 (left). Rnd3-p190RhoGAP helps bleb growth by suppressing RhoA activation and actin polymerization during the expansion phase. On the other hand, RhoA-ROCK1 promotes actin reassembly during the retraction phase and also removes Rnd3 from the plasma membrane by phosphorylating Rnd3. During apoptosis, bleb cycle is also regulated this double negative feedback loop between Rnd3-p190 RhoGAP and RhoA-ROCK1, but in the early stage of apoptosis, ROCK1 is activated by caspase-3 in a RhoA independent manner. Therefore, ROCK1 excludes Rnd3 from the plasma membrane and RhoA is more likely to be activated in the early stage of apoptosis, resulting in the acceleration of retraction of bleb and the reduction in the size of blebs. Caspase 3 also cleaves the C-terminal region of Xkr8, leading to constitutive activation of Xkr8. Due to the phospholipid scrambling activity of Xkr8, PtdIns(4,5)P2 together with PS in the inner leaflet of the plasma membrane translocates to the outer leaflet of the plasma membrane. At the late stage of apoptosis, due to the phospholipid scrambling by Xkr8, the amount of PtdIns(4,5)P2 in the inner leaflet decreases. Reduction of the amount of PtdIns(4,5)P2 prevents the formation of the actin cortex and inhibits cross-linking activity of Ezrin, leading to the formation of larger bleb. Fragmented cellular components and substances such as DAMPs now can translocate to the bleb to form a functional apoptotic body.

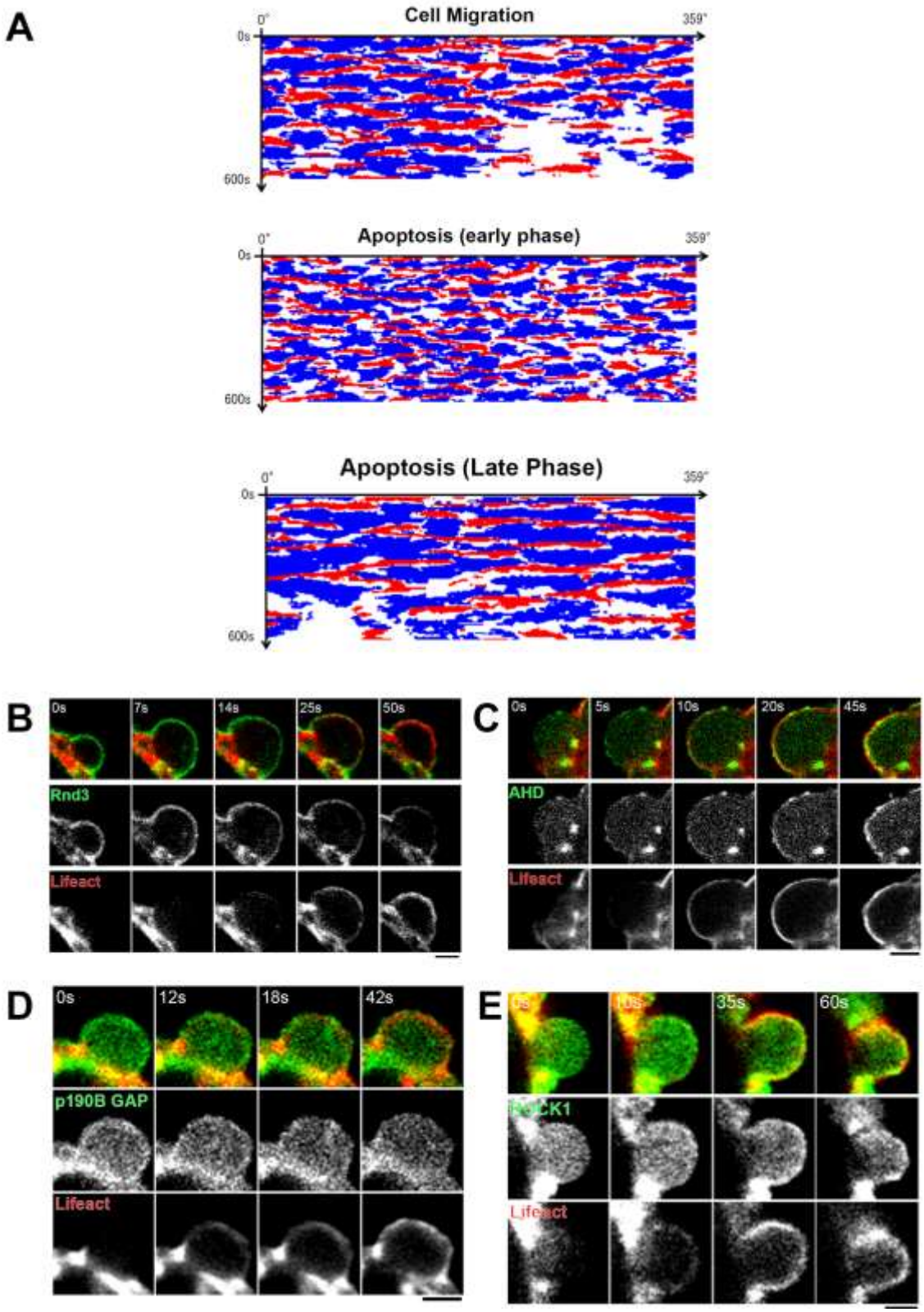
A
Cell Migration
0°
359°
0s
600s
Apoptosis (early phase)
0°
359°
0s
600s
Apoptosis (Late Phase)
0°
359°
0s
600s
B
0s
7s
14s
25s
50s
Rnd3
Lifeact
C
0s
5s
10s
20s
45s
AHD
Lifeact
D
0s
12s
18s
42s
p190B GAP
Lifeact
E
0s
10s
35s
60s
Lifeact

FigureS1. Distribution of Rnd3 and active RhoA in membrane blebs.

(A) Tricolor map of membrane blebs in freely-moving DLD1 cells (Cell Migration) and apoptotic DLD1 cells (early and late stage). Angular coordinates are shown on the horizontal axis, and time is shown on the vertical axis. Red zones represent expansion, blue zones represent retraction, and white zones represent no movement.

(B) Membrane blebbing of freely-moving DLD1 cells transfected with Lifeact–RFP and GFP-tagged Rnd3. The localization of Rnd3 at the plasma membrane gradually disappeared upon the initiation of the retraction of membrane blebs (t =25 s). Scale bar, 2 μm.

(C) Membrane blebbing of freely-moving DLD1 cells transfected with Lifeact–RFP and GFP-tagged Anillin homology dmain (AHD), which specifically binds to GTP form of RhoA. Scale bar, 2 μm.

(D) Membrane blebbing of freely-moving DLD1 cells transfected with Lifeact–RFP and GFP-tagged p190B RhoGAP. Scale bar, 2 μm.

(E) Membrane blebbing of freely-moving DLD1 cells transfected with Lifeact–RFP and GFP-tagged ROCK1. Scale bar, 2 μm.

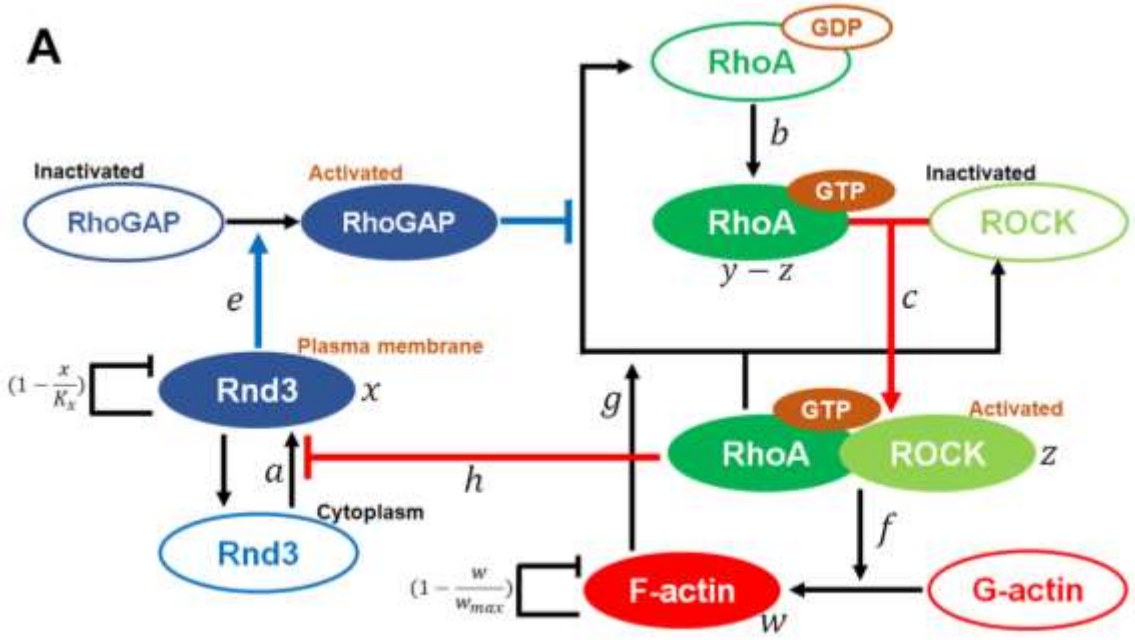

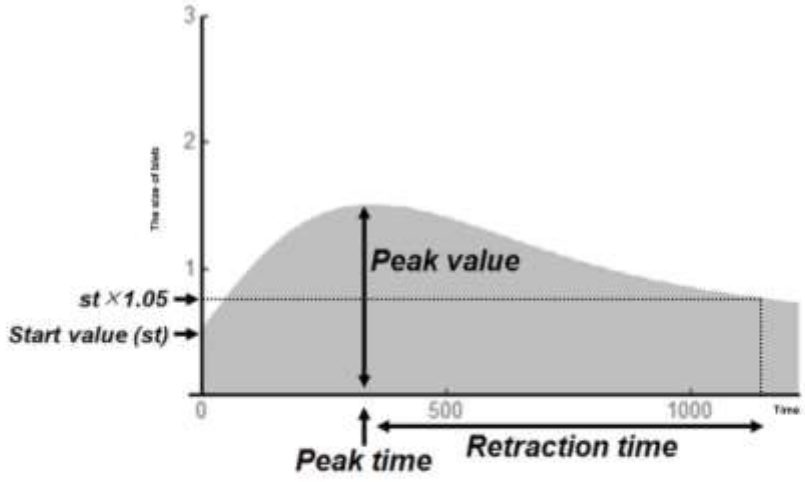

C

	a		*b*		*c*		*e*		*f*		*g*		*h*	
	×0.5	×2	×0.5	×2	×0.5	×2	×0.5	×2	×0.5	×2	×0.5	×2	×0.5	×2
Peak value	0.929121	1.115059	1.319694	0.818391	1.105361	0.944194	0.924151	1.30591	1.218533	0.839117	0.998163	1.00371	1.038989	0.9512
Peak time	0.840278	1.28125	1.663194	0.684028	1.1875	0.916667	0.833333	1.819444	1.326389	0.75	0.996528	1.013889	1.138889	0.8680
Retraction time	0.680851	2.91253	2.91253	0.541371	2.294326	0.862884	0.680851	2.335697	1.42435	0.723404	0.899527	1.36052	2.816785	0.6855

FigureS2. Construction of mathematical simulation on bleb dynamics

(A) The mathematical model of bleb dynamics was constructed based on the molecular networks of blebbing in freely-moving DLD1 cells as follows;

Equation (1)

$$\frac{dx}{dt} = (a - hzx)\left(1 - \frac{x}{K_x}\right) \quad (1a)$$

$$\frac{dy}{dt} = (b - (ex + gw)y) \quad (1b)$$

$$\frac{dz}{dt} = c(y - z) - (ex + gw)z \quad (1c)$$

$$\frac{dw}{dt} = fz\left(1 - \frac{w}{w_{max}}\right) \quad (1d)$$

$$\frac{dS}{dt} = -kwS + mp \quad (1e)$$

Equation (1a) represents the change in the amount of Rnd3 at the plasma membrane, *x*. Rnd3 is equally distributed at the plasma membrane at a constant concentration during the expansion phase (Fig.S1B). Therefore, we assume that Rnd3 is supplied to the plasma membrane from the cytoplasm at a constant rate *a*. Rnd3 was assumed to be removed at a rate, *hzx,* proportional to the concentration of active ROCK1 (*z*) and Rnd3 itself (*x*). This reflects the fact that Rnd3 is phosphorylated by active ROCK1 and sequestered in the cytoplasm via binding to 14-3-3. We assume that there is an upper limit to the amount of Rnd3 at the plasma membrane (K_x) because the area of plasma membrane of the expanding blebs is restricted.

Equation (1b) represents the change in the amount of active RhoA at the plasma membrane, *y*. We assume that RhoA changes from an inactive state to an active state at a constant rate, *b*. Here we assume most RhoA are inactivated and reside at the plasma membrane because RhoA is tethered to the plasma membrane via lipid modification (31) (Fig.S1C). RhoGEFs activate RhoA at rate *b*. RhoA changes from an active state to an

inactive state at a rate of ($ex + gw$) y. It undergoes inactivation in proportion to the amount of Rnd3, x. This corresponds to the fact that Rnd3 activates p190-Rho-GAP and p190-Rho-GAP inactivates RhoA (Figs.S1B and S1D). We assumed that p190-Rho-GAP inactivates RhoA regardless of its binding to ROCK1. We also assume the inactivation occurring at rate proportional to the amount of actin at the plasma membrane, w, because components of mature actin cortex recruit Rho-GAPs, such as FilGAP (32).

Equation (1c) represents the change in the amount of active ROCK1 at the plasma membrane, z. Active ROCK1 increases at a rate of $c(y\text{-}z)$, which means that active ROCK1 increases in proportion to the amount of active RhoA that is not yet bound to ROCK1 (Figs.S1B and S1E). Considering that ROCK1 binds to RhoA on a one-to-one basis and maintains its activity while binding, the amount of active ROCK1, z, is equal to the amount of RhoA already bound to ROCK1. Therefore, the amount of active RhoA that can activate ROCK1 is described as (y-z). RhoA changes from an active state to an inactive state at a rate of ($ex + gw$) z, which reflects the fact that ROCK1 is inactivated when Rnd3 and actin inactivate RhoA bound to ROCK1.

Equation (1d) represents the change in the amount of actin filaments at the plasma membrane, w. Based on our previous observations, phosphorylation of Ezrin by ROCK1 is essential for reassembly of the actin cytoskeleton during the retraction phase of membrane blebs (Aoki et al. 2016). The amount of actin at the plasma membrane increases in proportion to the amount of active ROCK1 localized to the membrane at a rate of fz. Here we assume that only a subset of Ezrin is activated and that most of Ezrin is inactivated at the cytoplasm. In other words, the rate of activating Ezrin by ROCK1 is much smaller than the rate of inactivating Ezrin. From this assumption, active Ezrin does not decrease by binding to actin due to its rapid replenishment from the inactive Ezrin pool. Then we can consider the increase rate of actin as proportional to the amount of active ROCK1. As with Rnd3, we assume the amount of actin on membrane does not increase infinitely and the maximum value is set to $w_{\max}$

Equation (1e) represents the change in the surface area of bleb, S. The surface area of bleb increases at rate mp proportional to the intracellular pressure p. Conversely, the

surface area of bleb decreases in proportion to the amount of actin on membrane, *w*, and surface area itself, *S.* This represents the surface tension of the bleb surface, the strength of which is proportional to the amount of actin *w*.

(B) The three metrics that characterize bleb behavior were defined as follows; *Peak value* indicates the size of bleb when bleb expanded most; *Peak time* indicates the time when bleb expanded most; and *Retraction time* indicates the time taken for bleb to retract from the peak size to a size 1.05 times that at time = 0.

(C) The changes in three metrics when the value of each parameter was either doubled or halved. This table shows the ratio of the value of each cases to that of standard case. Parameter *a* indicates the rate at which Rnd3 is supplied to the plasma membrane. It is predicted from simulation that the size of bleb and the time taken for retraction increase as the value of *a* increases. This is because the increase of *a* upregulates the amount of Rnd3 at the plasma membrane (*x*), which in turn inhibits activation of RhoA-ROCK1 pathway according to equations (1b) and (1c), resulting in the delay of actin accumulation and thus bleb retraction.

Parameters *b* and *c* are functionally related and they account for the rate of RhoA activation and ROCK1 activation by RhoA, respectively. Increasing Parameter *b* upregulates RhoA activity at the plasma membrane (*y*) and subsequently ROCK1 activity (*z*), the rate of which is Parameter *c*. Since both parameters promote actin reassembly and accelerate the onset of retraction phase, the simulation predicts that the bleb size and the time taken for retraction decrease as *b* and *c* increase.

Parameter *h* stands for the rate at which Rnd3 activity is inhibited by ROCK1. When phosphorylated by ROCK1, phosphorylated Rnd3 is removed from the plasma membrane. Since increasing *h* downregulates the amount of Rnd3 at the plasma membrane (*x*), according to the equation (1a), the simulation predicts that blebs become smaller as the value of *h* increases, which results in the activation of RhoA-ROCK1 pathway.

Parameter *e* represents the rate of RhoA inhibition by RhoGAP. If the value of *e* is increased, RhoA activity at the plasma membrane (*y*) and ROCK1 activity (*z*) decreases. Therefore, it is predicted by the simulation that an increase of value *e* leads to the formation

of larger blebs.

Parameter f indicates the rate at which actin polymerizes as a consequence of activating the RhoA-ROCK1 pathway. Although this parameter is also difficult to modulate experimentally, the simulation predicts that the increasing f causes the upregulation of the amount of actin at the plasma membrane (w) and downregulation of bleb size (S).

Parameter g shows the rate at which RhoA is inhibited by actin filaments. When the value of g is increased, RhoA activity at the plasma membrane (y) and ROCK1 activity (z) decreases. Therefore, it is predicted that increase of g, the value of which cannot be experimentally controlled, leads to the formation of larger blebs.

Parameter k indicates the rate at which bleb expansion decelerates due to the elasticity of the cell membrane as the surface area of the bleb increases. Parameter mp represents the internal pressure of the cell. If the value of k is increased or if the value of mp is decreased, the bleb size (S) decrease.

We chose values of parameters used for figures in the main text as follows. We estimated the model parameters based on experimental data and regenerated the time series of abundances of four different molecules in the model (Rnd3, RhoA, ROCK1, and actin). We noted that the measurements of the absolute abundance of each molecule includes errors more than the temporal pattern. In parameter fitting, we focused on the temporal pattern of the abundance of molecules rather than their absolute abundances. For this purpose, we normalized the abundance of each molecule by setting the largest and the smallest values to be 1 and 0, respectively. We then recorded the representative time when the normalized values were 0.1, 0.2, … 0.9.

We also noted considerable variation of timing of the process between Bleb events. To cope with this, we divided the times obtained by the time when normalized abundance of actin was 0.5. We used these empirical values for parameter fitting of the model.

To reduce the number of parameters in the model, we introduced the following non-dimensional variables and parameters:

$$\hat{x} = \frac{x}{K_x}, \qquad \hat{y} = \frac{y}{b}, \qquad \hat{z} = \frac{z}{b}, \qquad \hat{w} = \frac{w}{w_{max}}, \tag{S1}$$

$$\hat{a} = \frac{a}{K_x}, \qquad \hat{h} = bh\,, \qquad \hat{e} = eK_x, \qquad \hat{f} = \frac{bf}{w_{max}}, \qquad \hat{g} = w_{max}g,$$

Then equations can be rewritten as the following four differential equations expressed in terms of these converted variables and parameters only:

$$\begin{aligned} \frac{d\hat{x}}{dt} &= \left(\hat{a} - \hat{h}\hat{z}\hat{x}\right)(1 - \hat{x}) \\ \frac{d\hat{y}}{dt} &= 1 - (\hat{e}\hat{x} + \hat{g}\hat{w})\hat{y} \\ \frac{d\hat{z}}{dt} &= c(\hat{y} - \hat{z}) - (\hat{e}\hat{x} + \hat{g}\hat{w})\hat{z} \\ \frac{d\hat{w}}{dt} &= \hat{f}\hat{z}(1 - \hat{w}) \end{aligned} \qquad \text{(S2).}$$

We generated time series of variables for a range of parameter values, and calculated the temporal patterns of four molecules in the same manner applied to the empirical data explained above. We searched for the parameter values that generate time series close to the empirical data. We adopted the Nelder-Mead Method for exploring best-fitting parameter set. We repeated the procedure 100 times with initial parameter set chosen randomly within the range of 0.01 to 1 and we identified the parameter set which has the smallest squared error. The values of the best fitted parameters are as follows; $\hat{a}$ = 2.496, c = 8.438, $\hat{h}$ = 15.928, $\hat{e}$ = 3.619, $\hat{f}$ = 1.190, and $\hat{g}$ = 0.394.

Based on these calculations, parameters in the mathematical simulation were optimized based on measurement values obtained from experimental data. In the case of **freely-moving DLD1 cells (Standard case)**, each parameter was determined as follows; a=5, b=1, c=8.4, e=1.8, f=2.4, g=0.2, h=15.8, m=1, p=1, k=1, K_x=2, and $W_{\max}$=2.

In order to simulate **membrane blebs in early phase of apoptosis**, we modified the model as follows;

$$\frac{dx}{dt} = (a - h(z + z_c)x)\left(1 - \frac{x}{K_x}\right), \qquad \text{(2a)}$$

$$\frac{dw}{dt} = (fz + f_c z_c)\left(1 - \frac{w}{w_{max}}\right). \qquad \text{(2b)}$$

Here we assumed that there is another cascade for activating ROCK1 by caspase other than RhoA. z_c represents the amount of ROCK1 activated by caspase, and f_c represents

the rate at which activated ROCK1 promotes actin polymerization. The total amount of activated ROCK1 is $z+z_c$. We regarded z_c as a constant value because in the experiments the amount of ROCK1 activated by caspase does not change during apoptosis. The modified model showed that removal of Rnd3 from the plasma membrane and reassembly of actin cortex occurred earlier in the expansion phase as compared to the cell migration bleb model. Each parameter was determined as follows; a=5, b=1, c=8.4, e=1.8, f=2.4, g=0.2, h=15.8, m=1, p=1, k=1, K_x=2, W_{max}=2, $\boldsymbol{z_c}$ **=1**, and $\boldsymbol{f_c}$ **= 2.4**.

In order to simulate bleb dynamics when **ROCK1 is constitutively active at a constant level** regardless of the Rnd3-RhoGAP pathway, we used following parameters. Parameters are: $\boldsymbol{z}$**=2**, a=5, b=1, c=8.4, e=1.8, f=2.4, g=0.2, h=15.8, m=1, p=1, k=1, K_x=2, and W_{max}=2.

Acknowledgements

I’m deeply grateful to Prof. Y. Iwasa from Kwansei-Gakuin University and Dr. S. Satoi for constructing mathematical models of blebs and insightful discussion. I would like to sincerely thank Prof. S. Uchida and Mr. S. Harada for visualization and quantitative analysis of bleb dynamics.

I also extend my gratitude to all members of Ikenouchi laboratory for advice, discussion, and other many supports. I would like to thank Lecturer K. Matsuzawa for constructive discussion and advice. I would especially thank for Prof. J. Ikenouchi for supporting my study and student life.

A part of this research was supported by JSPS KAKENHI (17J00242) and a JSPS Research Fellowship for Young Scientists (DC1).

References

1. Nagata, S., and Tanaka, M. (2017). Programmed cell death and the immune system. Nature reviews. Immunology 17, 333-340.
2. Charras GT (2008) A short history of blebbing. J Microsc 231(3):466–478.
3. Shi, J., Zhao, Y., Wang, K., Shi, X., Wang, Y., Huang, H., Zhuang, Y., Cai, T., Wang, F., and Shao, F. (2015). Cleavage of GSDMD by inflammatory caspases determines pyroptotic cell death. Nature 526, 660-665.
4. Janicke, R.U., Ng, P., Sprengart, M.L., and Porter, A.G. (1998). Caspase-3 is required for alpha-fodrin cleavage but dispensable for cleavage of other death substrates in apoptosis. J Biol Chem 273, 15540-15545.
5. Zheng, T.S., Schlosser, S.F., Dao, T., Hingorani, R., Crispe, I.N., Boyer, J.L., and Flavell, R.A. (1998). Caspase-3 controls both cytoplasmic and nuclear events associated with Fas-mediated apoptosis in vivo. Proc Natl Acad Sci U S A 95, 13618-13623.
6. Coleman, M.L., Sahai, E.A., Yeo, M., Bosch, M., Dewar, A., and Olson, M.F. (2001). Membrane blebbing during apoptosis results from caspase-mediated activation of ROCK I. Nat Cell Biol 3, 339-345.
7. Sebbagh, M., Renvoize, C., Hamelin, J., Riche, N., Bertoglio, J., and Breard, J. (2001). Caspase-3-mediated cleavage of ROCK I induces MLC phosphorylation and apoptotic membrane blebbing. Nat Cell Biol 3, 346-352.
8. Caruso, S., and Poon, I.K.H. (2018). Apoptotic Cell-Derived Extracellular Vesicles: More Than Just Debris. Frontiers in immunology 9, 1486.
9. Paluch, E.K., and Raz, E. (2013). The role and regulation of blebs in cell migration. Curr Opin Cell Biol 25, 582-590.
10. Aoki, K., Maeda, F., Nagasako, T., Mochizuki, Y., Uchida, S., and Ikenouchi, J. (2016). A RhoA and Rnd3 cycle regulates actin reassembly during membrane blebbing. Proc Natl Acad Sci U S A.

11. Ikenouchi, J., and Aoki, K. (2017). Membrane bleb: A seesaw game of two small GTPases. Small GTPases 8, 85-89.
12. Tixeira, R., Phan, T.K., Caruso, S., Shi, B., Atkin-Smith, G.K., Nedeva, C., Chow, J.D.Y., Puthalakath, H., Hulett, M.D., Herold, M.J., and Poon, I.K.H. (2019). ROCK1 but not LIMK1 or PAK2 is a key regulator of apoptotic membrane blebbing and cell disassembly. Cell Death Differ.
13. Zhang, Q., Schepis, A., Huang, H., Yang, J., Ma, W., Torra, J., Zhang, S.Q., Yang, L., Wu, H., Nonell, S., Dong, Z., Kornberg, T.B., Coughlin, S.R., and Shu, X. (2019). Designing a Green Fluorogenic Protease Reporter by Flipping a Beta Strand of GFP for Imaging Apoptosis in Animals. Journal of the American Chemical Society 141, 4526-4530.
14. Wickman, G.R., Julian, L., Mardilovich, K., Schumacher, S., Munro, J., Rath, N., Zander, S.A., Mleczak, A., Sumpton, D., Morrice, N., Bienvenut, W.V., and Olson, M.F. (2013). Blebs produced by actin-myosin contraction during apoptosis release damage-associated molecular pattern proteins before secondary necrosis occurs. Cell Death Differ 20, 1293-1305.
15. Rao, L., Perez, D., and White, E. (1996). Lamin proteolysis facilitates nuclear events during apoptosis. J Cell Biol 135, 1441-1455.
16. Chardin P (2006) Function and regulation of Rnd proteins. Nat Rev Mol Cell Biol 7(1): 54–62.
17. Riou P, et al. (2013) 14-3-3 proteins interact with a hybrid prenyl-phosphorylation motif to inhibit G proteins. Cell 153(3):640–653.
18. Bovellan M, et al. (2014) Cellular control of cortical actin nucleation. Curr Biol 24(14): 1628–1635.
19. Ikenouchi, J. (2016). How do cells sense actin cortex-free membrane? Cell cycle (Georgetown, Tex.) 15, 2687-2688.
20. Suzuki, J., Denning, D.P., Imanishi, E., Horvitz, H.R., and Nagata, S. (2013). Xk-related protein 8 and CED-8 promote phosphatidylserine exposure in apoptotic cells. Science 341, 403-406.

21. Janmey, P.A., Bucki, R., and Radhakrishnan, R. (2018). Regulation of actin assembly by PI(4,5)P2 and other inositol phospholipids: An update on possible mechanisms. Biochem Biophys Res Commun 506, 307-314.
22. Varnai, P., and Balla, T. (1998). Visualization of phosphoinositides that bind pleckstrin homology domains: calcium- and agonist-induced dynamic changes and relationship to myo-[3H]inositol-labeled phosphoinositide pools. J Cell Biol 143, 501-510.
23. Sakuragi, T., Kosako, H., and Nagata, S. (2019). Phosphorylation-mediated activation of mouse Xkr8 scramblase for phosphatidylserine exposure. Proc Natl Acad Sci U S A 116, 2907-2912.
24. Mashima, T., Naito, M., and Tsuruo, T. (1999). Caspase-mediated cleavage of cytoskeletal actin plays a positive role in the process of morphological apoptosis. Oncogene 18, 2423-2430.
25. Segundo, C., Medina, F., Rodriguez, C., Martinez-Palencia, R., Leyva-Cobian, F., and Brieva, J.A. (1999). Surface molecule loss and bleb formation by human germinal center B cells undergoing apoptosis: role of apoptotic blebs in monocyte chemotaxis. Blood 94, 1012-1020.
26. Schiller, M., Bekeredjian-Ding, I., Heyder, P., Blank, N., Ho, A.D., and Lorenz, H.M. (2008). Autoantigens are translocated into small apoptotic bodies during early stages of apoptosis. Cell Death Differ 15, 183-191.
27. Zirngibl, M., Furnrohr, B.G., Janko, C., Munoz, L.E., Voll, R.E., Gregory, C.D., Schett, G., and Herrmann, M. (2015). Loading of nuclear autoantigens prototypically recognized by systemic lupus erythematosus sera into late apoptotic vesicles requires intact microtubules and myosin light chain kinase activity. Clinical and experimental immunology 179, 39-49.
28. Berda-Haddad, Y., Robert, S., Salers, P., Zekraoui, L., Farnarier, C., Dinarello, C.A., Dignat-George, F., and Kaplanski, G. (2011). Sterile inflammation of endothelial cell-derived apoptotic bodies is mediated by interleukin-1alpha. Proc Natl Acad Sci U S A 108, 20684-20689.

29. Schiller, M., Heyder, P., Ziegler, S., Niessen, A., Classen, L., Lauffer, A., and Lorenz, H.M. (2013). During apoptosis HMGB1 is translocated into apoptotic cell-derived membranous vesicles. Autoimmunity 46, 342-346.
30. Tucher, C., Bode, K., Schiller, P., Classen, L., Birr, C., Souto-Carneiro, M.M., Blank, N., Lorenz, H.M., and Schiller, M. (2018). Extracellular Vesicle Subtypes Released From Activated or Apoptotic T-Lymphocytes Carry a Specific and Stimulus-Dependent Protein Cargo. Frontiers in immunology 9, 534.
31. Mitin, N., Roberts, P.J., Chenette, E.J., and Der, C.J. (2012). Posttranslational lipid modification of Rho family small GTPases. Methods in molecular biology (Clifton, N.J.) 827, 87-95.
32. Saito, K., Ozawa, Y., Hibino, K., and Ohta, Y. (2012). FilGAP, a Rho/Rho-associated protein kinase-regulated GTPase-activating protein for Rac, controls tumor cell migration. Mol Biol Cell 23, 4739-4750.